Design of Wide Particle Size Range Aerodynamic ~~Inlet~~Injection System with New Pre-focus Structure

Junhong Huang [1], Lei Li [2,3], Xue Li [2,3], Zhengxu Huang [2,3] and Zhi Cheng[4]

[1]Guangdong MS institute of scientific instrument innovation, Guangzhou, 510632, China

[2]Institute of Mass Spectrometry and Atmospheric Environment, Jinan University, Guangzhou, 510632, China

[3]Guangdong Provincial Engineering Research Center for On-Line Source Apportionment System of Air Pollution, Guangzhou, 510632, China

[4]Institute of Systems Engineering, Academy of Military Sciences, Tianjin, 300161, China

Correspondence: Lei Li (lileishdx@163.com)

Abstract: A new aerodynamic ~~lens~~ injection system has been designed for wide particle size range, ~~which~~combining a new pre-focus structure, a smaller buffer chamber, a five-stage lens. Compared with previous injection systems, the new design adds virtual ~~impact~~impactors and pre-focus ~~structure on the basis of traditional PM2.5 lenses. The system has a small~~structures, while reducing the overall volume ~~and successfully improves~~ by 90 %. The newly developed pre-focus structure effectively addresses the challenges associated with the focusing ~~ability of traditional PM2.5 lens systems to 100 nm-10 μm. The structure of the new pre-focus hole solves the problem of affecting the~~ and transmission ~~and focusing~~ of large particles, ~~effectively~~ significantly reducing the beam width and dispersion angle of particles ~~entering~~exiting the critical hole, thus preventing the ~~virtual impactor, significantly improving~~buffer chamber from becoming excessively large. Furthermore, the focusing ~~effect of large particles, and enhancing the~~ capability and transmission efficiency ~~of~~for large particles~~. It can also effectively focus particles without~~ have been significantly ~~accelerating particles, avoiding~~enhanced, with the ~~structural size of the buffer chamber being too large~~transmission range expanded to encompass particles from 100 nm to 10 μm. Numerical ~~simulation shows~~simulations demonstrate that the ~~new~~ injection system can transmit particles ~~with 100 % efficiency in the range of 0.2-4 μm particles, and can achieve the transmission of~~ within the 1- to 9 μm ~~particles~~range with an efficiency ~~higher than~~exceeding 90 %. ~~The~~Additionally, the standard microsphere experiment verified the good consistency between the performance of the injection system and the simulation results. In the testing of standard ~~Arizona~~ dust, the wide-range particle size distribution obtained by the new injection system is highly consistent with Aerodynamic Particle Sizer (APS~~ 3321. The~~). In summary, this new ~~injection~~

system combines a new pre-focus structure, a smaller buffer chamber, a five-stage lens, and the whole injection system volume that is up to 90 % smaller than previous self-made wide-range lens designs. At the same time, itdesign has ultra-high transmission efficiency while reducing volume, demonstrating the potential for miniaturization potential of single particle aerosol mass spectrometer in detecting particles with a wide particle size range.

Keywords: Aerosol particles; Aerodynamic lens; Beam width; Transmission efficiency; Numerical simulation

1 Introduction

As a key component of aerosol mass spectrometry, the particle beam generator is used to focus the injected particles, and the focusing ability of the particle beam determines the detection sensitivity of the aerosol mass spectrometer. AsAerodynamic lenses, which are recognized as a commonwidely utilized particle beam focusing device, aerodynamic lensestechnology (Liu et al., 1995; Murphy et al., 2006; Zelenyuk et al., 2015; Clemen et al., 2020) utilize, leverage the inertia differencedifferential between particles and surrounding fluids to effectively focus particles and are widely used in different, finding extensive application across various aerosol mass spectrometry systems (Peck et al., 2016). In addition to its application in aerosol mass spectrometry, aerodynamic lens systems have also been appliedfound applications in many analytical equipmentinstruments. Researchers use aerodynamic lenses to introduce aerosol particles into pulsed X-ray beams and determine the particle composition using diffraction patterns and ion fragments generated when the X-ray pulse meets the particle (Loh et al., 2012). Aerodynamic lenses can also be used in the mass spectrometry of nano-mechanical resonators. They can achieveThe lenses enable efficient focusing and transmission and focusing of large analytes without the need for ionization, thus significantly improving theenhancing overall system performance of nano-mechanical mass spectrometers (Dominguez-Medina et al., 2018).

AlthoughWhile aerodynamic lenses havedemonstrate a significant transmission effect on particles, the most current designs primarily focus on a particle size range designed by most current aerodynamic lens is mainlythat falls within anthe same order of magnitude, and the size range that can be focused is mainly below 3μmwith effective focusing predominantly limited to particles smaller than 3 μm. (Fergenson et al., 2004; Srivastava et al., 2005; Tobias et al., 2006). SuchWe typically assess the particle transmission capacity of injection systems by considering the range where the transmission efficiency exceeds 50 %, such as the 25-250 nm of Liu et al. (Liu et al., 1995), the 100-900 nm and the 340-4000 nm of Schreiner et al. (Schreiner et al., 1998; Schreiner et al., 1999), the 60-600 nm of Zhang et al. (Zhang et al., 2004), and the 125-600 nm of Zelenyuk et al. (Zelenyuk et al., 2015). The particle size of atmospheric aerosols in the atmosphere rangesspans from sub-nanometer to millimeter level, and scales. Consequently, broadening the

particle focusing ~~sample injection of particles with a wide particle size~~ range is ~~crucial~~essential for ~~improving~~enhancing the analytical ~~ability~~capabilities of aerosol mass spectrometry, ~~such as~~particularly in the ~~analysis~~examination of biological aerosols, dust, and single cells.

Researchers have been actively working to ~~expand~~extend the particle transmission range ~~of particles~~ by optimizing aerodynamic lenses. Research has ~~shown~~found that the focusing performance of aerodynamic lenses for small particles below ~~50nm~~50 nm is limited by Brownian motion, while focusing ~~on~~of large particles is mainly affected by the larger inertia of particles (Wang et al., 2005; Wang and Mcmurry, 2006).

At present, most ~~of the~~ reported ~~aerodynamic~~ lenses ~~have low efficiency in transmitting large~~ transported large particles inefficiently(Cahill et al., 2014; Deng et al., 2008; Williams et al., 2013; Wu et al., 2009). The significant expansion of particle ~~size (Cahill et al., 2014; Deng et al., 2008; Williams et al., 2013; Wu et al., 2009), so the key to achieving simultaneous transmission with a wide particle size~~transport range ~~is to improve the focusing~~relies on the improvement of the transport performance of large particles~~. The~~, and the most direct ~~method~~way to achieve this goal is to increase the ~~stage~~ number of ~~lenses~~lens stages. For example, Lee et al.(Lee et al., 2013) designed a seven-stage lens for particle detection in the range of 30 nm to 10 μm, but this study does not consider the impact of critical ~~holes~~hole on the transmission loss of large particles and it is not applied in practice. Cahill et al. (Cahill et al., 2014) designed a high-pressure lens, and used a very long buffer chamber combined with a seven-stage lens to ~~transmit~~transport 4-10 μm particles. However, ~~experiments show that~~ the transmission efficiency of 4 μm and 9 μm particles ~~is~~in the experiment was only 20 %, and the overall size of the lens ~~system is~~was relatively large. Increasing the ~~stage~~ number of lens stages is obviously beneficial for expanding the transmission ~~of wide~~ range ~~particle size~~of particles, but it ~~can~~ also ~~lead to~~ brings disadvantages such as excessive ~~volume of the~~ injection system volume and increased assembly difficulty~~, as~~. As mentioned by Liu et al. (Liu et al., 2007) ~~mentioned~~ in ~~the~~their report ~~that~~, the beam focusing effect ~~will decrease with~~decreased as the ~~decrease in~~ assembly accuracy of the ~~aerodynamic~~ lens system decreased.

Hari et al. (Hari et al., 2007) added a virtual impactor behind the critical hole~~, and their study shows that using the virtual impactor structure can~~ to reduce ~~the~~ cross trajectory phenomenon of large particles, which ~~is~~was beneficial for ~~improving~~enhancing the transmission performance ~~of large particles in~~within the injection system. Chen et al. (Chen et al., 2007) ~~investigated~~studied the effect of the ~~front~~structural configurations before and ~~rear structure of~~after the critical hole on particle loss through numerical simulation and experimental verification~~, and optimized the structure to enhance~~. They improved the ~~transmission~~transport efficiency of particles ~~with 50nm and below, but~~that are 50 nm or smaller by optimizing the ~~transmission~~structure. However, the transport range ~~is~~did not significantly ~~extended~~expand. Liu et al. (Liu et al., 2007) ~~unified~~reduced the wall impact loss of particles by unifying the inner diameter of the downstream pipeline of the critical hole ~~to reduce the wall impingement loss of particles.~~. Additionally, Hwang et al. (Hwang

et al., 2015) proposed a ~~new type of~~novel convergent-divergent critical hole~~, which can~~ that effectively ~~reduce~~reduces the incident angle of large particle ~~beams through a converging-diverging structure design~~ and ~~achieve particle transmission~~transports particles in the range of 30 nm to 10 μm efficiently. However, ~~the~~due to technological limitations, this new type of critical hole is difficult to ~~fabricate due to the limitation of processing technology~~manufacture and has not yet been applied in practice. ~~The~~ In conclusion, the above ~~studies indicate~~research indicated that ~~the~~ large particles transmission in ~~the~~ aerodynamic lens ~~system loss~~systems experience significant losses on the surface of the critical ~~hole~~holes. Du et al. (Du et al., 2023) first proposed a pre-focus design ~~for the first time to address the shortcomings of loss caused by large particles hitting the surface of the critical hole. A~~ that includes a two-stage lens ~~is added~~positioned at the front of the critical hole~~, so that large~~. With the aid of this pre-focus structure, particles ~~could be focused on~~are effectively aligned along the axis ~~to a greater extent~~ before entering the critical hole. This design ~~greatly~~significantly reduces the ~~beam incident~~incidence angle of large particles ~~in front of the critical hole,~~ , thereby ~~reducing~~minimizing the impact loss ~~of large particles~~ on the surface of the critical hole. ~~Combined with the seven-stage lens, efficient transmission of 62 nm-13 μm particles is achieved.~~ However, due to the ~~acceleration~~ large divergence angle of particles after ~~passing through the pre-focus lens, their downstream divergence angle after leaving~~they exit the critical hole ~~is large. Therefore~~, it is ~~necessary~~essential to ~~match~~incorporate a buffer chamber with a diameter of 250 ~~mm to achieve efficient transmission of particles~~millimeters, along with a ~~wide particle size range mentioned above. This~~seven-stage lens system, to efficiently transport particles ranging from 62 nm to 13 μm. Nevertheless, this design ~~results in a very large~~ markedly increases the overall size of the injection system, which ~~is not conducive to~~poses challenges for the miniaturization of the mass spectrometer.

This ~~paper introduces~~study designs a ~~newly designed and manufactured~~new small~~-~~ volume pre-focus wide~~-~~ range aerodynamic lens injection system (PFW-ALens) for ~~transporting~~ particles with diameters ranging from 100 nm to 10 μm. The ~~key components of the~~ injection system ~~include~~consists of a novel ~~low-pressure loss~~ pre-focus ~~hole~~ structure, a small buffer chamber, and a five-stage aerodynamic lens ~~group. Computational~~. This study uses computational fluid dynamics software ~~is used~~ to ~~model~~simulate the transmission performance from the ~~sampling~~ inlet to the ~~nozzle~~vacuum chamber, and verifies it ~~is verified by~~through experiments. ~~Numerical~~The numerical simulation ~~shows~~results demonstrate that the particle transmission efficiency ~~of particles in the range of 100 nm-9 μm is higher~~is greater than 90~~%. In experimental verification, the transmission~~ % for sizes ranging from 100 nm to 9 μm. The results obtained from the experiments demonstrate significant consistency with the simulation outcomes, particularly revealing that efficiency ~~of particles in the range of 100 nm-5 μm is above 90 %, and the transmission efficiency of particles in the range of~~exceeds 50 % for particles up to 9 μm ~~and below is more than 50 %.~~. This ~~lens~~injection system has great potential for application in bioaerosol analysis, ~~sand and~~ dust analysis, and miniaturization of mass

~~spectrometers~~spectrometers.

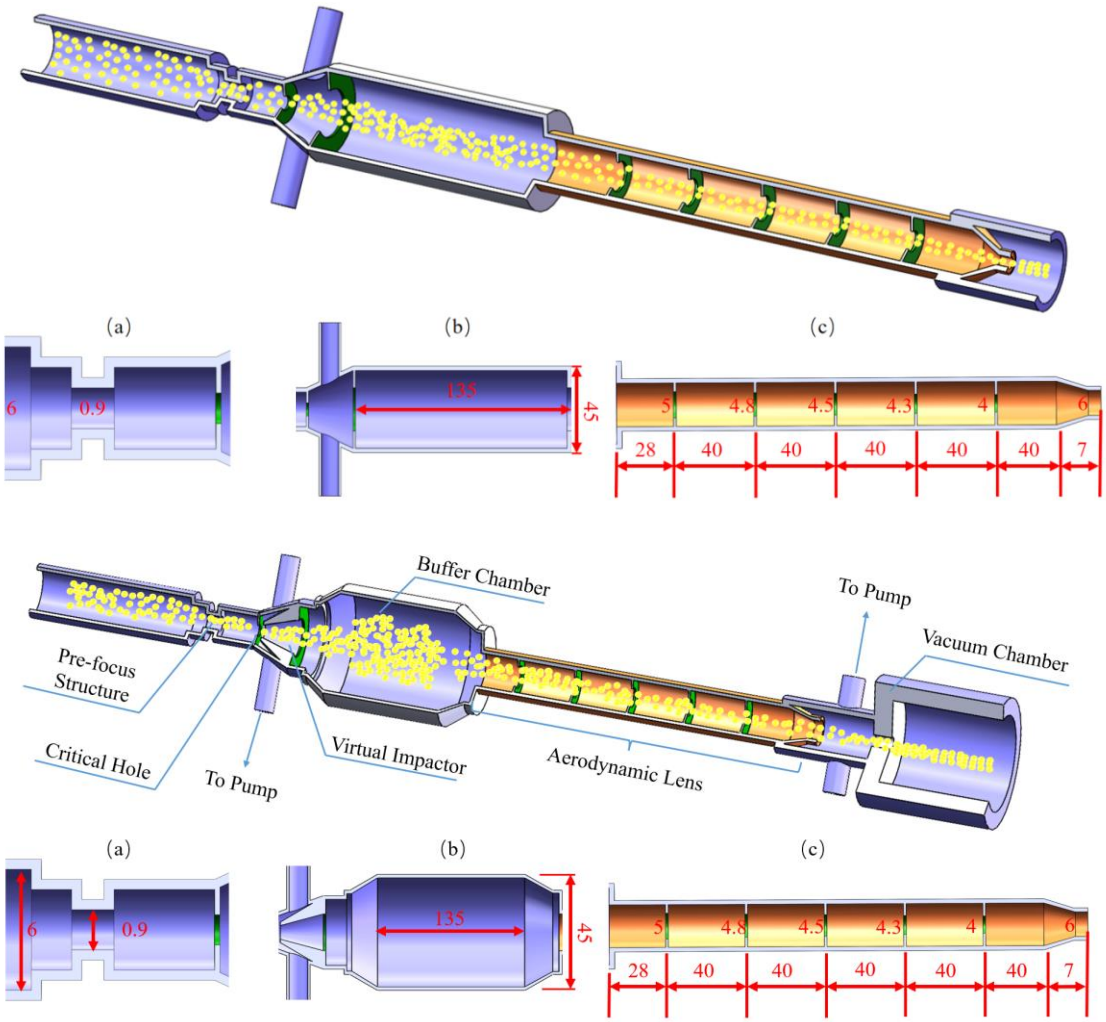

Fig. 1 Structural design of the injection system. Locally displayed are the pre-focus ~~hole~~structure (a), buffer chamber (b), and ~~aerodynamic~~five-stage lens system (c).

2 Numerical simulation and experimental design

2.1 Physical models

Fig. 1 shows the structure and key dimensions of the injection system, which consists of four modules~~, namely the~~: pre-focus ~~hole~~structure, the separation cone, the buffer chamber, and ~~the~~a five-stage aerodynamic ~~five-stage lens group. Fig. 1(a ~ c) respectively represent~~ lens. The distance from the inlet of the buffer chamber to the outlet of the acceleration nozzle in this study is 370 mm, compared to 570 mm in the injection system designed by Du et al. The particles are first focused near the axis with the aid of the pre-focus structure before passing through the critical ~~dimensions of each component. Aerosol particles approach the centerline through pre-focus holes, and~~hole, which has a diameter of 0.26 mm, at a flow rate of 640 mL/min. A separation cone ~~with diameter of 1mm and angle of 15 ° is set~~, located 1.6 mm downstream of the critical hole~~.~~, features

a diameter of 1 mm and an angle of 30 °. The excess air between the critical hole and the separation cone is extracted by a sidevacuum pump to achievecondense the concentration effect of aerosol particles, which then enter entering the buffer chamber. TheAs the high-speed particles acceleratedpass through the critical hole, they gradually decelerate inwithin the buffer chamber, and then are driven by the. The airflow then drives them into the aerodynamic lens system. The aerodynamic lens system consists of five apertures, which composed of holes with diameters of 5 mm, 4.8 mm, 4.5 mm, 4.3 mm and 4 mm, respectively, and an accelerating nozzle with a diameter of 3 mm. The length from the inlet of the buffer chamber to the outlet of the acceleration nozzle is 370 mm, and the distance between the same components in the injection system designed by Du et al. is 570 mm. The aerodynamic lens system consisting of different diameters of apertures canthat effectively focus aerosol particles within a certain range onto the axis of the lens. Finally, aerosolparticles onto the central axis within a specific range. In addition, this study utilized a smooth nozzle at the end of the aerodynamic lens. As mentioned by Zhang et al. (Zhang et al., 2004) in their study, this nozzle provides better collimation for small particles areand improves the transport efficiency of large particles compared to stepped nozzles. The particles focused by the lens group will be further accelerated into the vacuum chamber by the action of the accelerating nozzle and enter the subsequent diameter measurement system.

2.2 Numerical model

Ansys-Meshing is used to generate the mesh, and Fluent software is used to calculate the flow of gas and particle coupling between the sampling inlet and the accelerating nozzle.vacuum chamber. The pressure atboundary conditions for the sampling inlet is set to 101325 Pa, of the injection system, the outlet pressurepumping port of the virtual impactor is, and the outlet of the lens are set to 101325 Pa, 600 Pa, and 0.1 Pa, respectively. Under these conditions, the buffer chamber and the aerodynamic lens group used are both set to operate in an environment below 300 Pa, and the pressure at the outlet of the accelerating nozzle is 0.1 Pa. The parameter settings are consistent with the study of Zhang et al. (Zhang et al., 2002). In addition, the Viscous model used in the simulation is a laminar flow model. The discrete format of the flow equation is is employed for simulation, and the second-order upwind. The motion of aerosol particles will use the User Define Function (UDF) flow equation is selected as the discretization scheme. During the simulation, user-defined functions (UDFs) are utilized to load themodify and implement particle resistance modeldrag and the Brownian force model. By settingmodels, allowing for more accurate particle motion trajectories. Finally, the discrete phase model (DPM) is employed to define the number, diameter, and release position of the particles. Upon completion of the simulation, the trajectories and velocities of the particles in the DPM model, the trajectory and velocity of particles can beare obtained through cloud imagescontours.

2.3 Experimental exploration

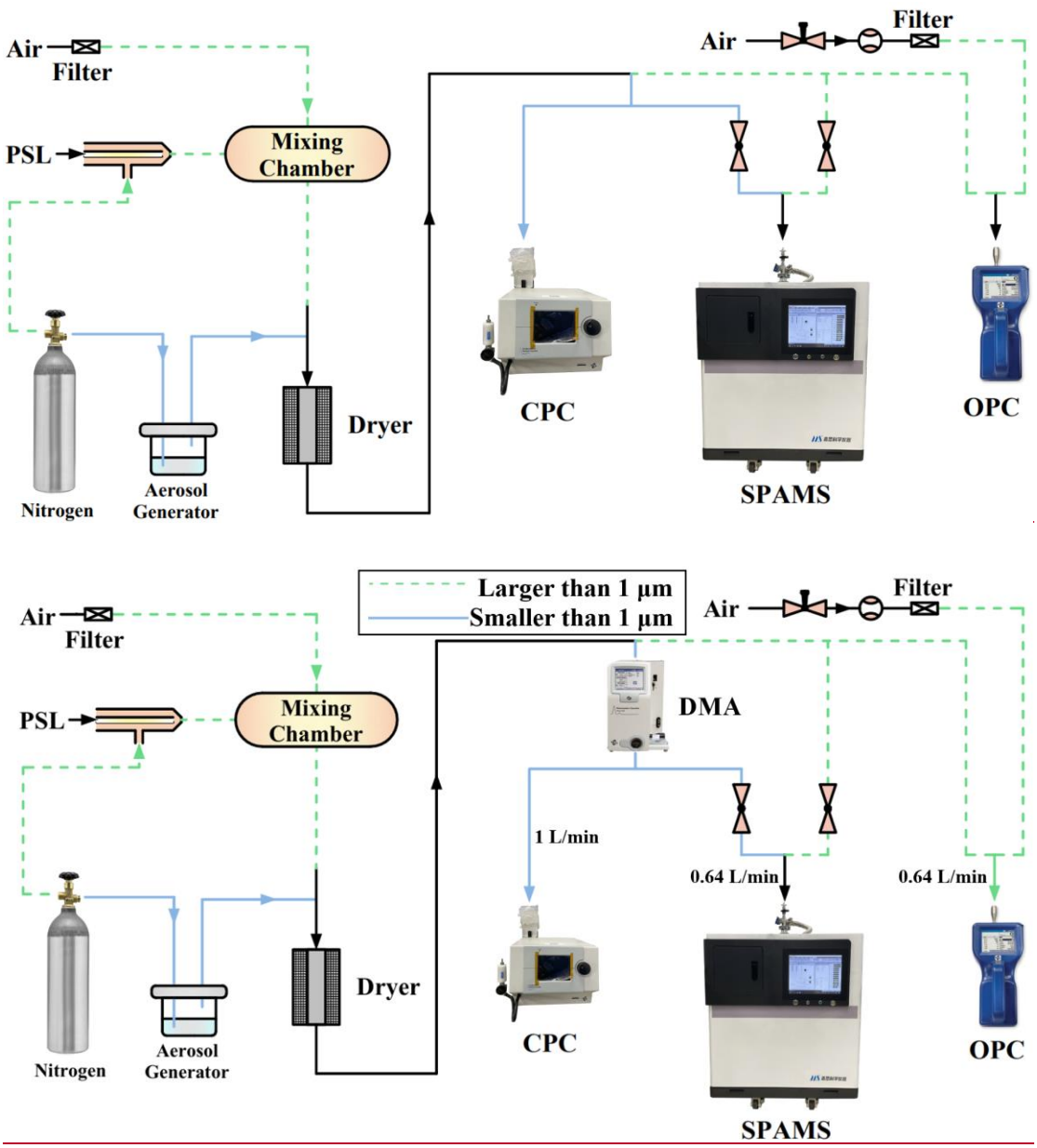

Fig. 2 Gas ~~path connection~~Path Connections and Flow Rates to Each Detector in ~~experiment~~Experiment

Standard polystyrene latex spheres (PSL, Thermo Fisher Scientific) ranging from 100 nm to 10 μm are used to characterize the focusing ability of aerodynamic lens system. The operation for generating and counting aerosols larger than 1 μm is as follows. ~~First~~Initially, the PSL solution is diluted with pure water, ~~and then~~after which nitrogen ~~is used~~serves as the carrier gas to atomize the PSL solution using an ICPMS atomizer ~~before passing it~~(Ge, C21-1-UFT02). The atomized mixture is subsequently directed into the mixing chamber, where the injection rates of the PSL solution and nitrogen are meticulously set to 10 μL/min and 0.2 L/min, respectively. The excess moisture in the atomized aerosol particles is removed by heating the mixing chamber and introducing a drying tube, and then the aerosol particles are introduced into the optical particle counter (OPC, TSI, Model 9306) and Bio-SPAMS respectively through a three-way tube for

counting. For particles ~~below~~smaller than 1 μm, an aerosol generator (TSI, Model 9302) is used to ~~generate~~produce aerosols. The generated aerosols are first sorted by a differential mobility analyzer (DMA, TSI, Model 3082) and ~~condensed~~then directed to a condensation particle counter (CPC, TSI, Model 3775) ~~is used~~and biological aerosol single particle mass spectrometer (Bio-SPAMS) for counting. ~~The specific~~ respectively. The detailed experimental gas path connection is shown in Fig. 2, where the blue solid line is the test pipeline connection scheme for the transmission efficiency of particles below 1 μm, and the green dotted line represents the test pipeline connection scheme for the transmission efficiency of particles above 1 μm. It is important to note that during the experiment, we utilized additional airflow. For experiments involving particles smaller than 1 μm, this additional airflow was implemented to address flow mismatches between the aerosol generator and the detection instruments. In experiments with particles larger than 1 μm, the additional airflow helped resolve the issue of unequal flow rates between the OPC and Bio-SPAMS, ensuring that the flow rates entering both instruments remained consistent during measurement.

~~The single particle mass spectrometer~~The Bio-SPAMS used in this study is similar to HP-SPAMS (Du et al., 2024), but its optical system has been improved. The first diameter measuring laser is designed ~~as~~with a beam ~~-~~-splitting optical structure similar to ~~APS3321, and~~that of the ~~dual~~APS 3321. The method involves using a beam ~~can measure~~splitter to divide the diameter measuring laser (Sony SLD3234VF) into two nearly parallel beams and calculating the aerodynamic diameter of the particles~~. Photomultiplier~~ by the time they pass through these beams. The photomultiplier tube ~~PMT is used to detect~~detects the number of particles passing through the laser~~.~~ by collecting light signals, and PMT 1-1 is used to count the number of particles passing through the first laser of the split beam. In the experiment, we ~~regard~~defined the total number of particles detected by PMT ~~detections obtained~~1-1 per unit time as the total number of particles entering Bio-SPAMS. For particles larger ~~than 1 μm, the particle count of the corresponding size in OPC is taken as the total number of particles of that size, and the transmission efficiency of that particle size is the~~ than1 μm, the ratio of the total number of particles entering ~~OPC and SPAMS, respectively.~~both Bio-SPAMS and OPC is used to determine the transmission efficiency. For particles ~~below 1~~smaller than1 μm, the transmission efficiency is calculated as the ratio of the particle concentration recorded by ~~PMT~~Bio-SPAMS to ~~the particle concentration~~that recorded by CPC.

3 Results and discussions

3.1 ~~Aerodynamic lens~~ Injection system with virtual ~~impact~~impactor

~~The basic model of aerodynamic lenses is consistent with that of~~Currently, the lens designed by Zhang et al. (~~Zhang et al., ~~2004)~~, as shown in Fig. 3. Simulation results of Zhang et al. show that the focusing range of the lens of this size is mainly between 50 nm and 3 μm, and the transmission efficiency of 1.5 μm is 50 %. The initial condition of this simulation is to assume that

~~particles are uniformly distributed from the buffer chamber to the front of the lens, but in fact, for large particles, the state of entering the lens is not the same. Many scholars~~, has been applied by numerous researchers (Canagaratna et al., 2007; Docherty et al., 2013; Drewnick et al., 2009; Meinen et al., 2010) ~~have used this lens system to carry out different studies, and added a buffer chamber and a virtual impactor structure as shown in Fig. 1(a) on the basis of this model.~~ across various fields. However, the simulation results presented by Zhang et al. indicate that the focusing range of such lenses primarily lies between 50 nm and 3 μm, with a transmission efficiency of 50 % at 1.5 μm, as illustrated in Fig. 3(a). Furthermore, Zhang et al. assumed in their simulations that particles were uniformly distributed from the buffer chamber to the area in front of the lens. In reality, however, the entry conditions for larger particles are not uniform. To gain further insights into the impact of this lens on particles within mass spectrometry instruments, this study enhances Zhang et al.'s model by incorporating a buffer chamber and a virtual impactor structure, as depicted in Fig. 1(b), and conducts relevant simulations for exploration.

Our team discovered that the virtual impactor used in this study is capable of transporting 100 nm particles downstream with an efficiency of over 90 %, with only a small fraction of particles being pumped away. This indicates that nearly all of the particles examined in this research can pass through the virtual impactor and be effectively transported downstream. In order to further compare the effects of the virtual impactor and pre-focus structure with the five-stage lens employed in this study, this study first removed the virtual impactor and pre-focus structure from Fig. 1 and simulated the transmission efficiency of the model (represented by the blue left triangle line). Subsequently, the virtual impactor (orange diamond line, original design) and the pre-focus structure (black square line, present design) were sequentially reintroduced to observe the enhancements in transmission efficiency. By comparing the transmission effects of three design above, the advantages of the design in Fig. 1 are highlighted.

The transmission efficiency presented in this study is the ratio of the number of particles at a distance of 110 mm from the lens outlet to the number of particles at the inlet of the injection system. The beam width of the particles is determined by selecting the radial distribution of 90 % of the particles at this same distance. The reason for choosing the 110 mm position is that it is downstream of all lasers, allowing for a clearer evaluation of the particle transport and focus effect.

By comparing the particle transmission efficiency curves before and after adding a virtual impactor, it can be found that after the addition of the virtual impactor (orange diamond symbol line), the focusing ability of the injection system for particles larger than 1 μm has increased to varying degrees, and the transmission efficiency of 7 μm particles has increased from the original 5 % to 30 %. Although the aerodynamic lens system with virtual ~~impact structure~~impactor has increased its ability to focus on large particles, this particle size range is still insufficient for the detection of large particle ~~aerosols~~ such as dust and organisms.

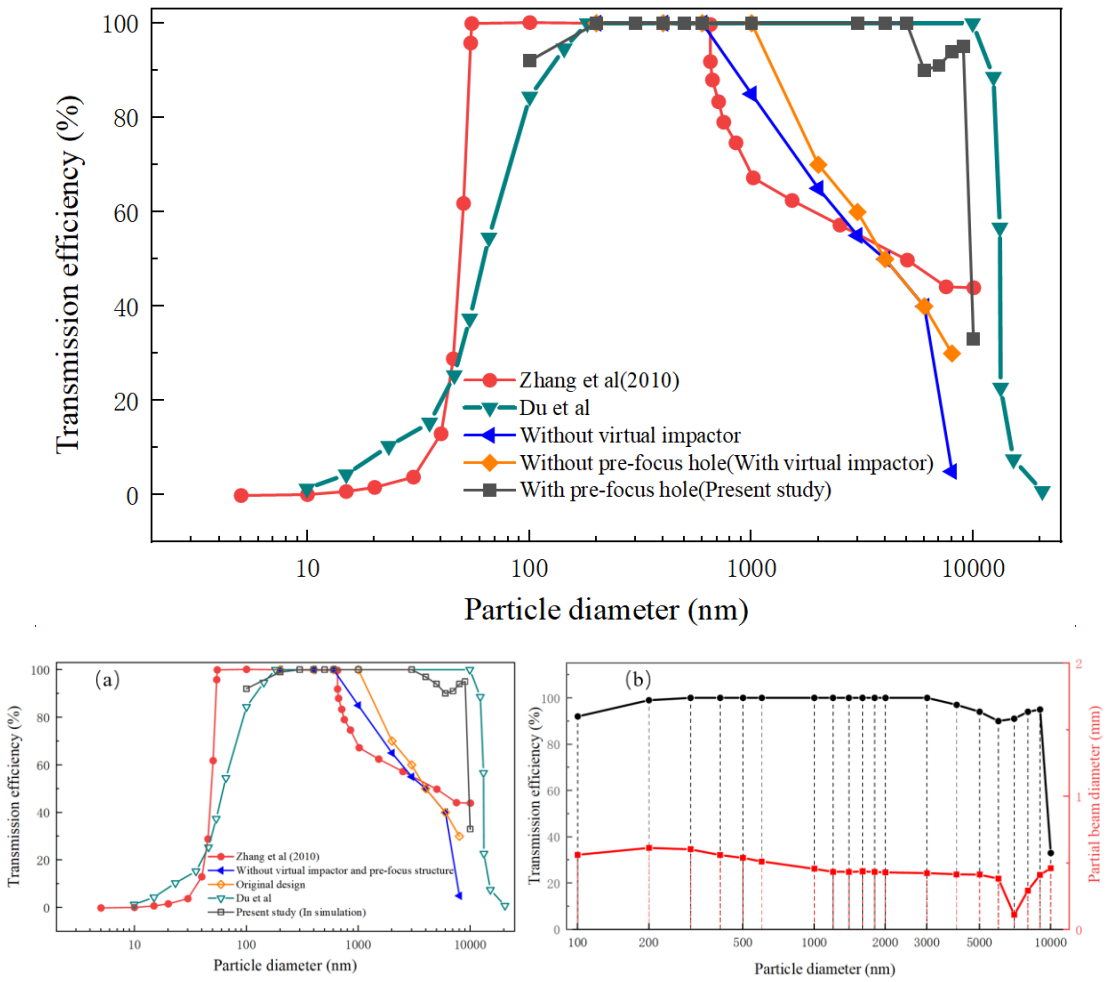

Fig. 3 ~~Curves~~Performance of ~~particle focusing ability for~~ different injection systems in simulation. Fig. 3 (a) shows the particle focusing range of different injection systems, and Fig.3 (b) shows the transmission efficiency and particle beam width of the injection system in this study (PFW-ALens) in terms of simulation.

~~3.2 Pre-focus~~ 3.2 Injection system with pre-focus structure

Du et al. ~~In response to the shortcomings~~proposed a pre-focus technique that incorporates a set of two-stage lenses in front of the critical hole to address the low efficiency of transporting larger particles mentioned in section 3.1 ~~regarding the transmission range of particles and the low transmission efficiency of larger particles,~~. From Fig. 3(a), it can be observed~~Du et al. pointed out that an important reason for the loss of large particles is~~ that ~~particles hit the surface of the critical hole to form the wall impingement loss. They proposed a pre-focus injection technique, which involves placing a set of two-stage lenses in the~~ the pre-focus injection ~~tube in front of the critical hole. The lenses can focus the particles to the axis in advance, avoiding the wall impingement loss of particles. This structure~~ system designed by Du et al. can reduce the loss of 10 μm particles from ~~the original~~ about 40 % to 0~~. The curve in Fig. 3 shows that the seven-stage aerodynamic~~

~~lens system with pre-focus structure designed by Du et al. can achieve~~ %, achieving efficient ~~transmission in a wide particle size~~ transport within the range of 0.18-10 μm. Although ~~the lens of~~ Du et al.'s injection system can ~~achieve~~cover a wide range~~, the~~ of particle sizes, there are still some drawbacks to the overall ~~lens~~ system ~~still has shortcomings~~. The main problem is that the particle beam diverges ~~greatly~~significantly after passing through the critical hole and the hole of virtual ~~impact hole, so~~impactor. Therefore, a ~~large~~ buffer with a diameter of 250 ~~mm~~millimeters and a height of 250 ~~mm~~millimeters is needed to ~~release~~accommodate all particles in the study.

Fig. ~~full~~4 compares the radial width of the particle ~~size range. Combined~~beams for 0.5 μm, 1 μm, 3 μm, and 5 μm particles at different positions in the original design, Du et al.'s design, and the design proposed in this study. Compared to the original design, the pre-focus structures designed by Du et al. and the one proposed in this study both reduce the radial width of the particle beams at the critical hole, the inlet of the virtual impactor, and the outlet of the nozzle. It is worth noting that the pre-focus structure designed by Du et al. significantly increases the radial distribution of the particle beam in the buffer cavity when transmitting large particles such as 3 μm (fig. 4(iii)) and 5 μm (fig. 4(iv)). This poses higher requirements for the focusing of the aerodynamic lenses located behind the buffer chamber, and a common approach to achieve this is to use additional stages of lenses for improved focusing. When combined with ~~the~~a seven-stage aerodynamic lens, the overall ~~size~~dimensions and volume of the ~~lens~~injection system can reach a diameter of 278 ~~mm~~millimeters and a height of 875 ~~mm. This is mainly because the design of the pre-focus lens produces a pressure loss, and the particles are focused on the central axis while also obtaining a large acceleration, which probably increases the divergence of the particles entering the strong buffer. As shown in~~millimeters. ~~Fig. 4, it can be found that the pre-focus structure makes the particles of different sizes accelerated compared with other systems. It can be found in Fig. 5(b) that the dispersion angle of 5 μm particles is also very large after leaving the critical hole, so a particularly large buffer chamber is needed to achieve particle collection and deceleration before entering the lens system to complete focusing.~~ A large-~~size~~sized injection system is not only detrimental to the miniaturization of mass ~~spectrometers~~spectrometers, but ~~also a~~the seven-stage lens ~~system~~ can also lead to ~~the increase of~~increased assembly ~~accuracy, and~~complexity, making it difficult to ensure the consistency of the ~~lens is difficult to ensure~~lenses.

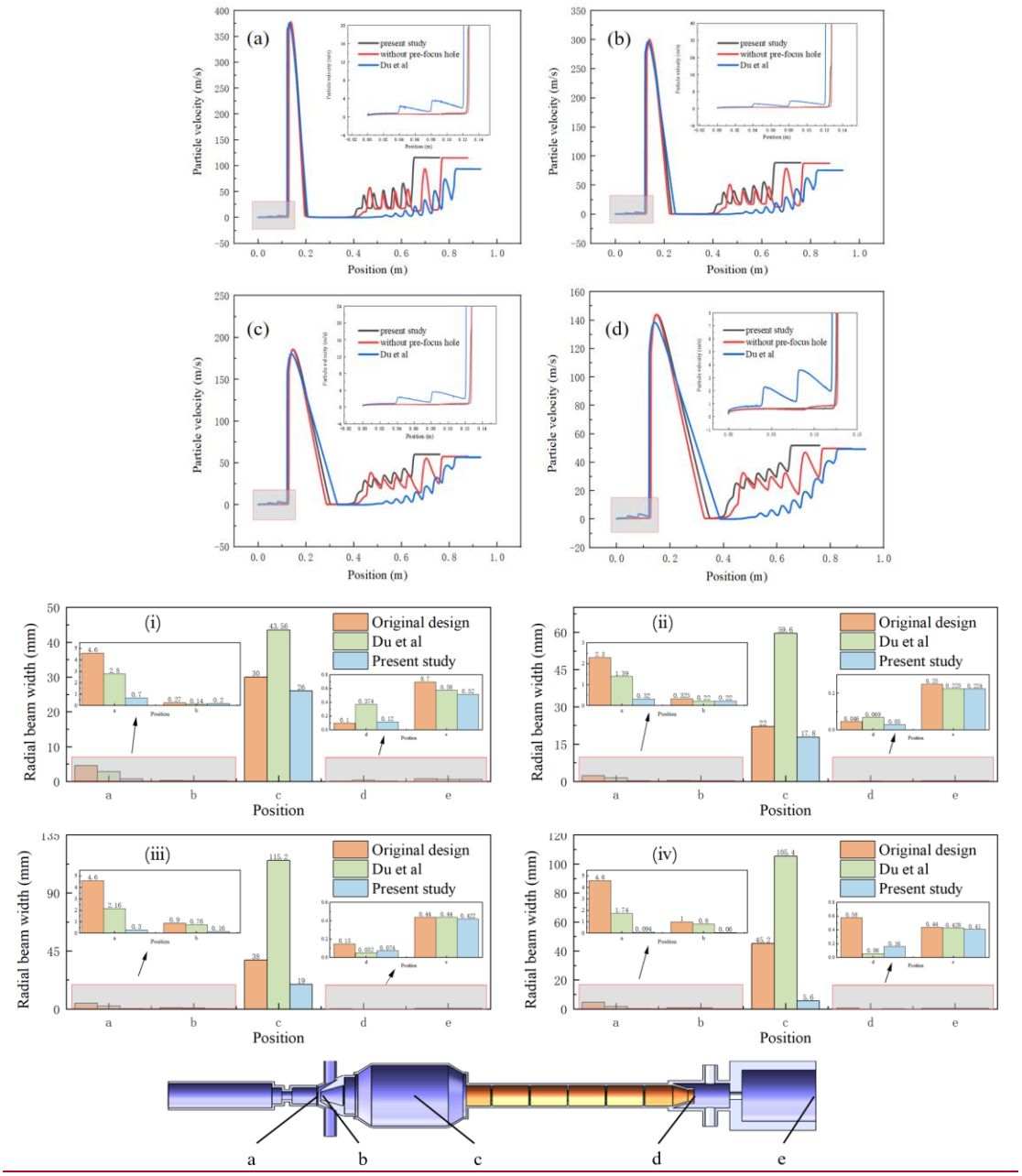

Fig. 4 Comparison of the radial width of the particle beam in the key components of the original design, Du et al.'s design, and the pre-focus injection system proposed herein. The particles characterized are 0.5 μm, 1 μm, 3 μm, and 5 μm, as represented by (i) to (iv), respectively. Specifically, (a) denotes the front end of the critical hole, (b) refers to the inlet of the virtual impactor, (c) designates the buffer chamber, (d) indicates the outlet of the acceleration nozzle, and (e) represents the outlet of the vacuum chamber.

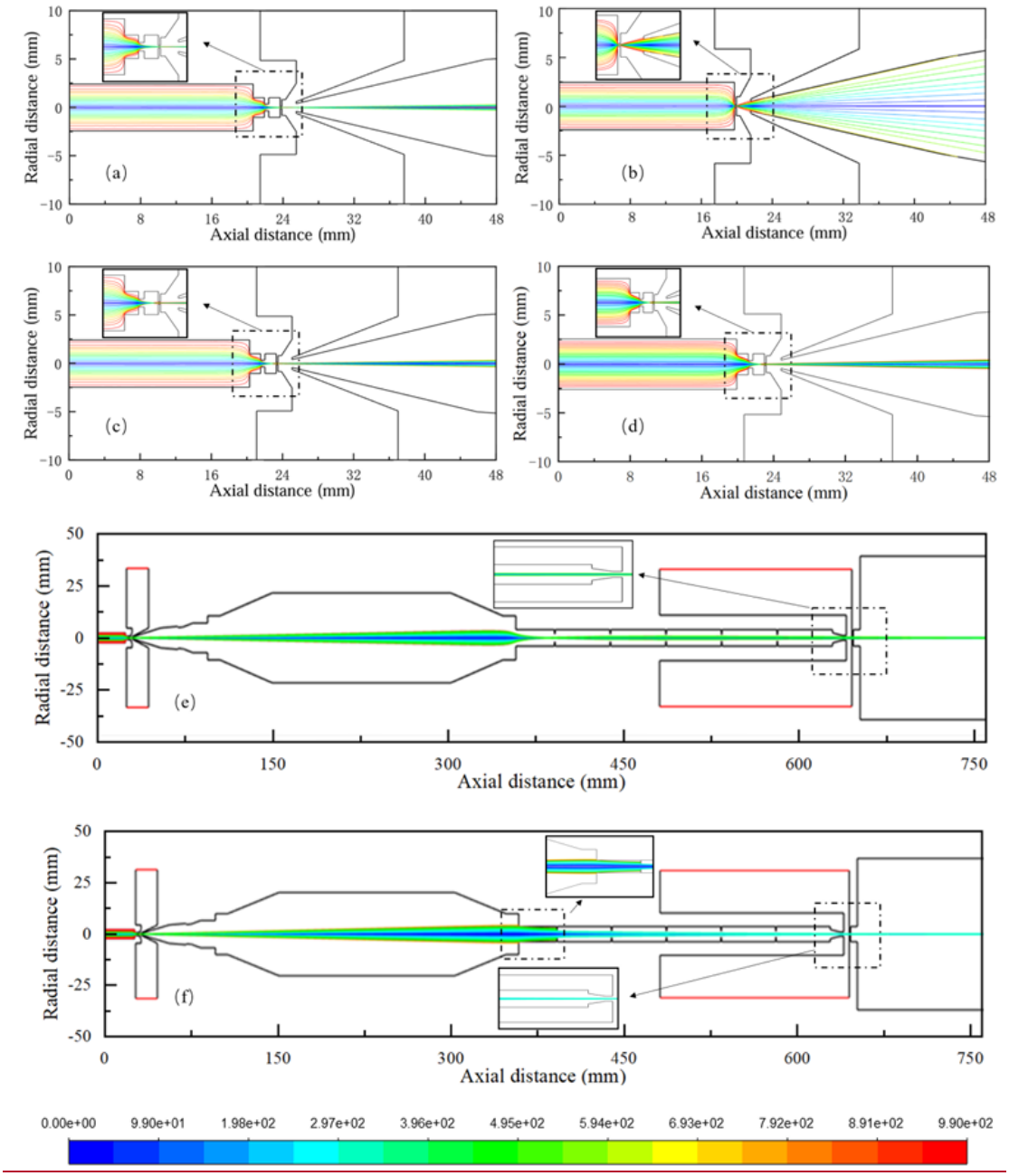

Fig. 4 Axial velocity of particles in different injection systems. (a) ~(d) represent particles of 0.5 μm, 1 μm, 3 μm, and 5 μm, respectively

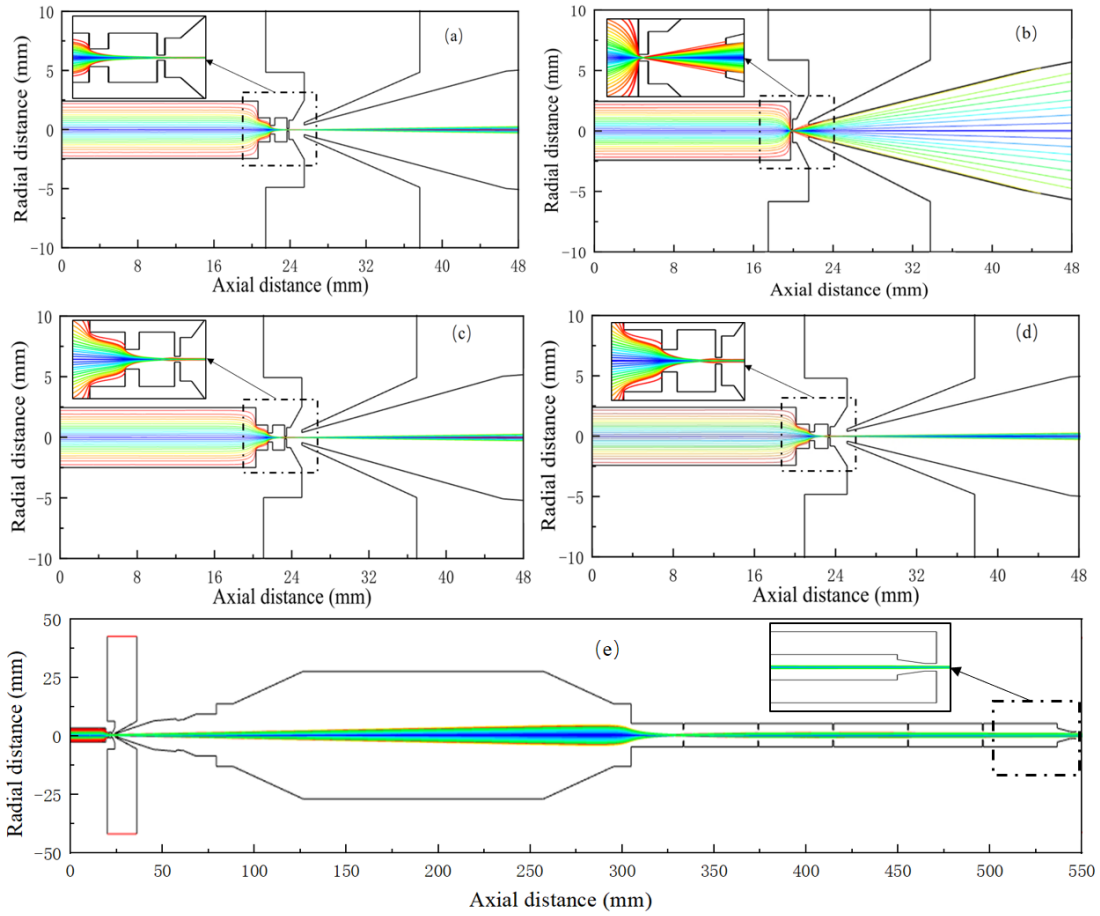

Fig.5 The trajectories of large particles in various injection systems are as follows: (a) shows the trajectory of 5 μm particles in the current design; (b) depicts the trajectory of 5 μm particles in the original design; (c) illustrates the trajectory of 8 μm particles in the current design; (d) presents the trajectory of 10 μm particles in the current design; (e) and (f) display the trajectory distributions of 8 μm and 10 μm particles within the overall injection system, respectively.

~~Fig. 5 Trajectories of large particles in different injection systems. (a) and (b) represent particle of 5 μm in the new and old systems, and (c) represents particle of 6 μm in the new system. (d) and (e) represent local and global trajectory of 8 μm~~

3.3 New design

~~In~~Section 3.2 examines the implications of the pre-focus structure proposed by Du et al. on increase in radial width, which directly pertain to the dimensions of the buffer chamber and the focusing efficiency of the particles. To mitigate these challenges, this study~~,~~ introduces a ~~new~~ single-stage ~~pre-focus structure is designed, which is equivalent to the critical hole as a two-stage~~ lens~~. The specific structural dimensions are shown in Fig. 1. In the previous text, the~~ pre-focus structure ~~of Du will lead to~~, with specific dimensions detailed in Fig. 1.

As illustrated in Fig. 4, the sample injection system equipped with the PFW-ALens demonstrates a significantly reduced radial width of the particle ~~acceleration and large dispersion~~

~~angle, which will directly affect the size of the buffer chamber~~ beam at various positions when transmitting particles of different diameters, compared to both the original design and the ~~focusing ability of the lens group. Therefore, the pressure drop of the~~ pre-focus structure ~~and the dispersion angle of particles are required in the~~ proposed by Du et al. Notably, at the buffer chamber, the beam width in this design ~~process. As shown in~~ decreases by 70 % to 95 % compared to Du et al.'s configuration. Furthermore, the radial~~Fig. 4, the velocity~~ distribution of ~~0.5 μm, 1 μm, 3 μm, and 5 μm particles under three different systems is compared. It can be found that the acceleration effect of~~ particles in the buffer chamber exhibits an inverse correlation with particle size, a phenomenon not observed in previous pre-focus ~~structure of Du is obvious, while the acceleration effect of the new pre-focus structure on particles is almost the same as that without the pre-focus structure.~~designs. This ~~means that the pre-focus hole used by PFW-ALens achieves pre-focus of large particles without additional acceleration effect on particles, which is more conducive to reducing the degree of change in the subsequent injection system. This also~~ finding provides a ~~good~~solid foundation for optimizing the lens system's length ~~of the lens system~~ and reducing the number of lenses required.

The ~~beam~~ divergence angle of the beam after particles ~~after passing~~pass through the critical hole directly ~~affects~~influences the design of the buffer chamber and the transmission efficiency of the particles ~~(Lee et al., 2013). The~~(Lee et al.,2013). A greater ~~the~~degree of divergence ~~degree, the easier it is for~~ increases the likelihood of particles ~~to collide~~colliding with the ~~pipeline wall and cause~~ walls, leading to losses, which has been a limitation in previous injection system designs. Fig. ~~. Therefore, the divergence angle after the critical hole determines the transmission range and efficiency of particles, especially for large particles. Fig. 5 shows~~5 illustrates the advantages of the ~~new pre-focus structure for the transmission of large~~proposed PFW-ALens in transmitting larger particles. Fig. ~~5a~~5(a) and ~~Fig. 5b represent~~5(b) depict the transmission trajectories of 5 μm particles in the PFW-ALens and the ~~injection~~original design system ~~without pre-focus holes~~, respectively. It can be observed that in the original design, the divergence ~~of~~significantly increases after the particles ~~after passing~~pass through the critical hole ~~is much greater in the structure without pre-focus, so it is necessary to adapt to a larger buffer chamber. Even the buffer chamber structure used by the pre-focus lens structure of Du et al. reaches 250 mm * 250 mm~~, resulting in collisions with the virtual impactor and subsequent losses. Conversely, Fig. 5(c) and 5(d) show the trajectories of ~~. Fig.~~5c and Fig. 5d show that even for larger particles ~~of 6 μm and~~(such as 8 μm~~,~~ and 10 μm) in the PFW-ALens ~~can maintain a very small~~ , revealing that the divergence angle~~. In fact, the structural size of the buffer chamber we used~~ after leaving the critical hole is ~~45 * 135 mm, and the volume of the buffer chamber is reduced by more than 90 % compared~~markedly small, leading to ~~the previous one.~~ a narrow beam widththroughout the entire system. This is in stark contrast to the results obtained using the pre-focus structures designed by Du et al. Furthermore, the dimensions of the buffer chamber used in this study are 45×135 mm, which

represents over a 90 % reduction in volume compared to the buffer chamber designed by Du et al.

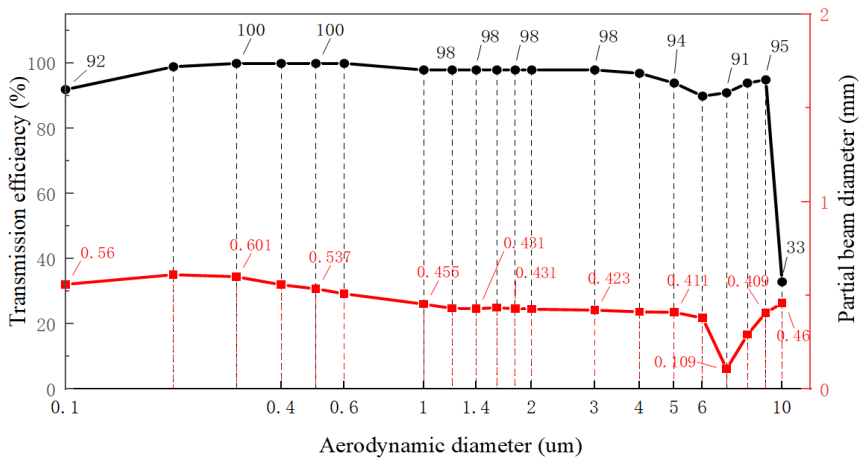

Fig. 6 Transmission efficiency and particle of new injection system

The overall transmission characteristics of the lens model are simulated, and the transmission efficiency is obtained by calculating the ratio of the number of particles at the sampling inlet and the outlet of the nozzle. The beam width is obtained by exporting the radial distribution coordinates of particles 110 mm downstream of the nozzle using Fluent software and then calculating its 90 % quantile. It can be seen from Fig. 6 that the particle transmission range of PFW-ALens is greatly increased, maintaining a transmission efficiency of over 90 % for particles in the range of 100 nm to 9 μm, until the transmission efficiency of 10 μm particles shows a cliff-like decline. At the same time, the simulation results show that the beam width can be kept below 0.6 mm

Fig. whole 3(b) demonstrates a significant enhancement in the particle size transmission range. In fact of the PFW-ALens. Within the particle size range of 100 nm to 9 μm, the transmission efficiency of remains above 90 %, with a notable decline in efficiency only observed for 10 μm particles. Furthermore, simulation results indicate that the beam width can be further increased by improving the structure. Simulation results show that maintained at less than 0.6 mm across the entire range of particle sizes. Additionally, the laser employed in this study differs from that utilized by Du et al.; the former has a laser beam diameter of 3 mm, suggesting that the diameter of the particle beam is considerably smaller than that of the laser beam. However, simulations also reveal that design improvements, such as increasing the length of the buffer chamber, can greatly improvefurther enhance the above efficiency, so the efficient transmission of 9 μm is efficiency for 10 μm particles, indicating that the effective transmission of 9 μm particles does not represent the upper limit of this system. In generalOverall, the particle focusing ability exhibited by capability of the PFW-ALens for particles in the 10 μm range of 10 μm is almost consistent withnearly comparable to the focusing performance ofobserved by Du et al. inwithin the same detectiontransmission range. It is worth notingIt's noteworthy that the lens model used in this study isemploys a PM2.5 five-stage lens, while in contrast to the seven-stage lens commonly

used in most ~~of the~~ wide-range ~~lenses generally use the structure of seven-stage lenses.~~injection systems. This ~~shows~~suggests that the ~~pre-focus device used~~injection system utilized in this study can ~~not only focus large particles more~~ effectively~~, but also accomplish focusing~~ focus larger particles with fewer lenses, thereby significantly reducing the overall volume of the injection system. This advancement is of ~~great significance~~significant importance for the miniaturization of ~~high-performance~~ single-particle mass ~~spectrometer.~~spectrometers.

3.4 Validation and application

Fig. ~~7~~6 compares the transmission efficiency of particles with different particle sizes in numerical simulation and experimental validation of PFW-~~Alens. It can be found that the~~ ALens. The results indicate a strong correlation between the experimental ~~verification results are basically in good agreement with the~~ findings and the numerical ~~simulation in~~ predictions. Within the ~~whole~~ particle size range~~. The actual test~~ of 200 nm to 6 μm, the measured transmission efficiency ~~of 200 nm - 6 μm particles can be maintained at more than~~ remains above 90~~%, and the actual test of 100 nm particles can also reach more than 87 %. In fact, 100nm particles will also cause some measurement loss~~ %. However, for 100 nm particles, the experimental results reveal substantial losses. This discrepancy is primarily due to the use of a dual-peak signal by the Bio-SPAMS for particle counting; to accommodate the requirements of biological fluorescence detection, the intensity of the second beam must be reduced, resulting in lower light scattering intensity~~.~~ for 100 nm particles, which in turn hinders accurate counting.

For particles ~~with a particle size greater~~larger than 6 μm, the testing ~~effect shows~~results show a ~~significant~~marked decrease in transmission efficiency~~, but~~. Nevertheless, 9 μm particles can still ~~remain above~~ maintain an efficiency of over 65 %. The trend ~~of~~in transmission efficiency for 10 μm particles is consistent with the simulation results, ~~with a transmission efficiency of~~ registering only 25 ~~%. The decrease in efficiency of large particles may be attributed to inconsistent transmission losses of particles between OPC and B-SPAMS.~~% efficiency.

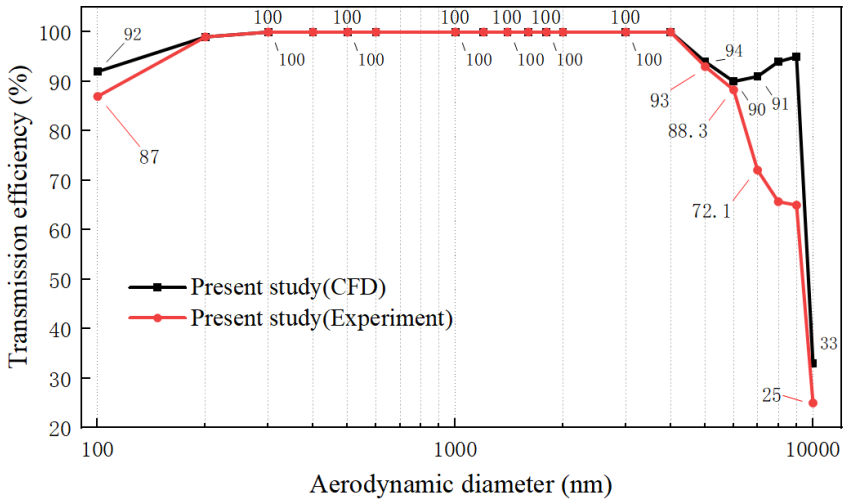

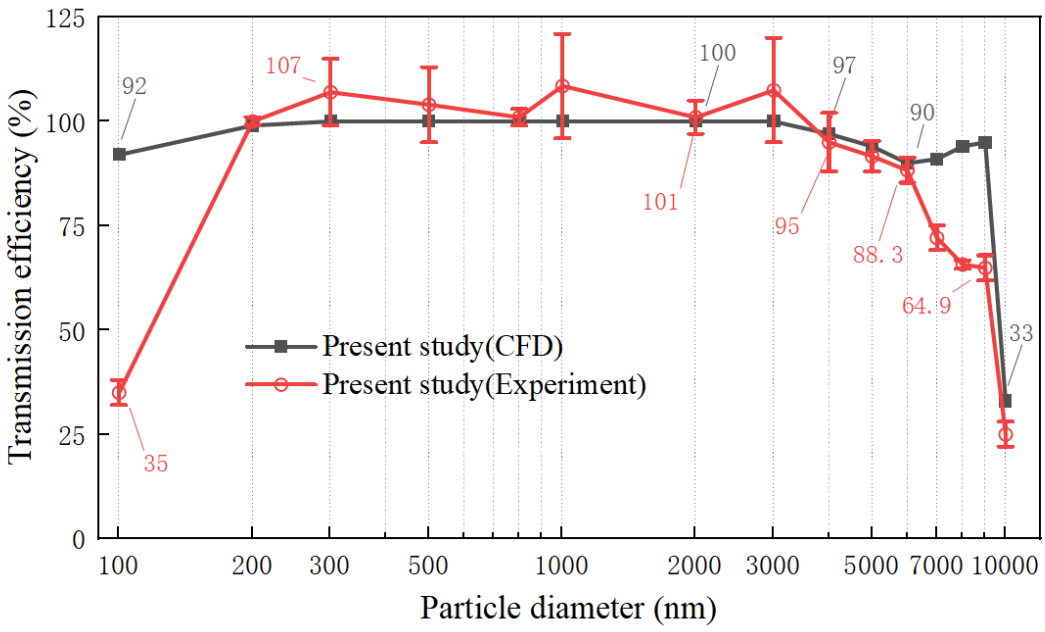

Fig. ~~7~~6 Experimental verification of particle transmission

~~In order to~~To characterize the analytical ~~ability~~capabilities of the PFW-ALens for large particles, ~~the~~ standard ~~ULTRAFINE TEST DUST from Arizona is~~ultrafine dust (ISO 12103, PTI) was selected as the test sample. ~~Firstly~~Initially, APS ~~is used~~was employed as the standard to detect the dust~~ as a standard,~~. Subsequently, tests were conducted and ~~then~~compared using the PFW-ALens ~~with pre-focus holes ((~~the red ~~dotted~~dashed line) and ~~injection systems without pre-focus holes (~~the original system (the black solid line~~) are used for testing and comparison.~~). The specific particle size distribution is ~~shown~~illustrated in Fig. ~~8, and~~7, where the Y-axis represents the normalized dN/dlogD. It is evident that the particle size distribution ~~measured by~~obtained using the PFW-ALens ~~is closer to~~closely aligns with that measured by the APS. The above experiments not only prove that PFW-ALens can more accurately detect the particle size distribution of dust compared to injection systems without pre-focus ~~holes~~structure, but also prove that PFW-ALens can achieve efficient transmission of large particles, demonstrating the potential of new lens structure in detecting large particle analysis.

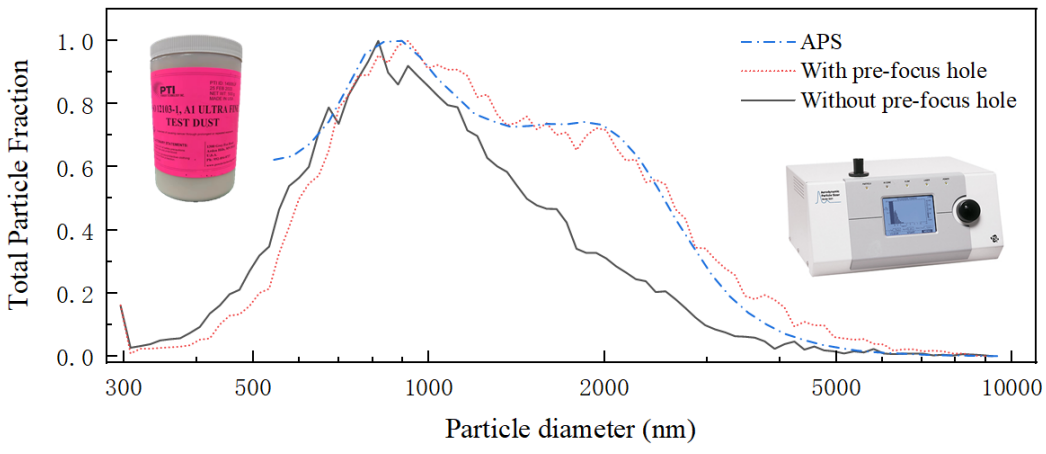

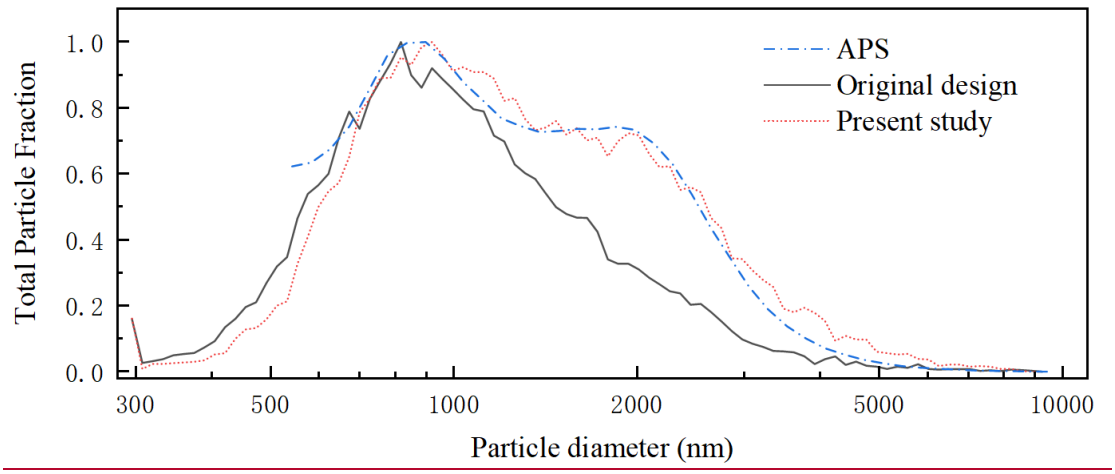

Fig. ~~8~~7 3-Minutes Average Particle ~~size distribution~~Size Distribution of ~~standard dust in different injection systems~~Standard Dust Across Different Injection Systems

5 Conclusions

In order to ~~improve~~enhance the transmission efficiency of large particles ~~in~~within the Bio-SPAMS injection system ~~and reduce the volume of the injection system,~~ while reducing its overall size, this study has developed ~~an~~a novel injection system, the PFW-ALens ~~with the ability~~, designed to focus large particles. This injection system ~~adopts~~incorporates a new pre-focus structure, which ~~can~~ effectively ~~reduce~~minimizes the ~~size~~dimensions of the buffer chamber and the number of lenses compared to ~~the injection system with~~ traditional pre-focus ~~holes, while maintaining~~injection systems, such as the work by Du et al. Furthermore, it maintains a low-loss transmission ~~effect~~performance for ~~particles with~~ a ~~larger~~wide range of particle ~~size range~~sizes. By ~~adding a~~ integrating the pre-focus structure, the focusing ~~ability~~capability of the ~~2.5 μm~~five-stage lens system ~~is~~has been significantly improved to accommodate particles up to 10 μm.

The numerical simulation results ~~show~~indicate that the ~~newly designed injection system can achieve the~~ PFW-ALens is capable of focusing and ~~transmission of~~ transmitting particles ~~with particle~~within the size ~~ranging from~~range of 100 nm ~~to 10~~to10 μm. ~~Among them~~Notably, the beam width of ~~large~~larger particles significantly decreases after ~~leaving~~exiting the separation cone ~~is significantly reduced compared to existing injection systems, which has extremely high particle transmission efficiency.~~, a phenomenon not previously observed in earlier studies. The ~~results show~~findings reveal that when particle sizes are less than 9 μm, the transmission efficiency can ~~be higher than~~exceed 90 ~~% when the particle size is less than 9 μm.~~%. Particles ~~with a~~within the range of 200 nm ~~-~~ to 4 μm ~~have~~demonstrate a transmission efficiency of 100 %. The injection system designed in this ~~paper is currently the one that~~study achieves the ~~widest~~broadest particle size range and the highest transmission efficiency ~~in the same~~among systems with similar structural ~~size~~dimensions. This innovative design is ~~beneficial for~~conducive to further reducing the structural size of the injection system and the number of aerodynamic lenses, ~~which provides ideas and inspiration~~providing a foundation for the miniaturization of ~~the~~ mass

~~spectrometers~~spectrometers.

Data availability. These data can be publicly accessible in free.

Author contributions. LL and ZXH designed the study; JHH and XL performed the simulations and experiments; JHH, LL, XL, ZXH and ZC participated in data analysis and result discussion; JHH and LL wrote the paper with the input from all authors.

Competing interests. The authors declare that they have no conflict of interest.

Financial support. This research was funded by the National key research and development program for young scientists (2022YFF0705400) and the Fundamental Research Funds for the Central Universities (21623205) .

References

Cahill, J. F., Darlington, T. K., Wang, X., Mayer, J., Spencer, M. T., Holecek, J. C., Reed, B. E., and Prather, K. A.: Development of a High-Pressure Aerodynamic Lens for Focusing Large Particles (4–10 μm) into the Aerosol Time-of-Flight Mass Spectrometer, Aerosol Science and Technology, 48, 948-956, 10.1080/02786826.2014.947400, 2014.

Canagaratna, M. R., Jayne, J. T., Jimenez, J. L., Allan, J. D., Alfarra, M. R., Zhang, Q., Onasch, T. B., Drewnick, F., Coe, H., Middlebrook, A., Delia, A., Williams, L. R., Trimborn, A. M., Northway, M. J., DeCarlo, P. F., Kolb, C. E., Davidovits, P., and Worsnop, D. R.: Chemical and microphysical characterization of ambient aerosols with the aerodyne aerosol mass spectrometer, Mass Spectrometry Reviews, 26, 185-222, 10.1002/mas.20115, 2007.

Chen, S.-C., Tsai, C.-J., Wu, C.-H., Pui, D. Y. H., Onischuk, A. A., and Karasev, V. V.: Particle loss in a critical orifice, Journal of Aerosol Science, 38, 935-949, 10.1016/j.jaerosci.2007.06.010, 2007.

Clemen, H.-C., Schneider, J., Klimach, T., Helleis, F., Köllner, F., Hünig, A., Rubach, F., Mertes, S., Wex, H., Stratmann, F., Welti, A., Kohl, R., Frank, F., and Borrmann, S.: Optimizing the detection, ablation, and ion extraction efficiency of a single-particle laser ablation mass spectrometer

for application in environments with low aerosol particle concentrations, Atmospheric Measurement Techniques, 13, 5923-5953, 10.5194/amt-13-5923-2020, 2020.
Deng, R., Zhang, X., Smith, K. A., Wormhoudt, J., Lewis, D. K., and Freedman, A.: Focusing Particles with Diameters of 1 to 10 Microns into Beams at Atmospheric Pressure, Aerosol Science and Technology, 42, 899-915, 10.1080/02786820802360674, 2008.
Docherty, K. S., Jaoui, M., Corse, E., Jimenez, J. L., Offenberg, J. H., Lewandowski, M., and Kleindienst, T. E.: Collection Efficiency of the Aerosol Mass Spectrometer for Chamber-Generated Secondary Organic Aerosols, Aerosol Science and Technology, 47, 294-309, 10.1080/02786826.2012.752572, 2013.
Dominguez-Medina, S., Fostner, S., Defoort, M., Sansa, M., Stark, A.-K., Halim, M. A., Vernhes, E., Gely, M., Jourdan, G., Alava, T., Boulanger, P., Masselon, C., and Hentz, S.: Neutral mass spectrometry of virus capsids above 100 megadaltons with nanomechanical resonators, Science, 362, 918-922, 10.1126/science.aat6457, 2018.
Drewnick, F., Hings, S. S., Alfarra, M. R., Prevot, A. S. H., and Borrmann, S.: Aerosol quantification with the Aerodyne Aerosol Mass Spectrometer: detection limits and ionizer background effects, Atmos. Meas. Tech., 2, 33-46, 10.5194/amt-2-33-2009, 2009.
Du, X., Zhuo, Z., Li, X., Li, X., Li, M., Yang, J., Zhou, Z., Gao, W., Huang, Z., and Li, L.: Design and Simulation of Aerosol Inlet System for Particulate Matter with a Wide Size Range, Atmosphere, 14, 10.3390/atmos14040664, 2023.
Du, X., Xie, Q., Huang, Q., Li, X., Yang, J., Hou, Z., Wang, J., Li, X., Zhou, Z., Huang, Z., Gao, W., and Li, L.: Development and characterization of a high-performance single-particle aerosol mass spectrometer (HP-SPAMS), Atmos. Meas. Tech., 17, 1037-1050, 10.5194/amt-17-1037-2024, 2024.
Fergenson, D. P., Pitesky, M. E., Tobias, H. J., Steele, P. T., Czerwieniec, G. A., Russell, S. C., Lebrilla, C. B., Horn, J. M., Coffee, K. R., Srivastava, A., Pillai, S. P., Shih, M.-T. P., Hall, H. L., Ramponi, A. J., Chang, J. T., Langlois, R. G., Estacio, P. L., Hadley, R. T., Frank, M., and Gard, E. E.: Reagentless Detection and Classification of Individual Bioaerosol Particles in Seconds, Analytical Chemistry, 76, 373-378,

571 10.1021/ac034467e, 2004.
572 Hari, S., McFarland, A. R., and Hassan, Y. A.: CFD Study on the Effects
573 of the Large Particle Crossing Trajectory Phenomenon on Virtual
574 Impactor Performance, Aerosol Science and Technology, 41, 1040-1048,
575 10.1080/02786820701697549, 2007.
576 Hwang, T.-H., Kim, S.-H., Kim, S. H., and Lee, D.: Reducing particle
577 loss in a critical orifice and an aerodynamic lens for focusing aerosol
578 particles in a wide size range of 30 nm — 10 μm, Journal of Mechanical
579 Science and Technology, 29, 317-323, 10.1007/s12206-014-1238-4, 2015.
580 Lee, K.-S., Hwang, T.-H., Kim, S.-H., Kim, S. H., and Lee, D.:
581 Numerical Simulations on Aerodynamic Focusing of Particles in a Wide
582 Size Range of 30 nm–10 μm, Aerosol Science and Technology, 47, 1001-
583 1008, 10.1080/02786826.2013.808737, 2013.
584 Liu, P., Ziemann, P. J., Kittelson, D. B., and McMurry, P. H.: Generating
585 Particle Beams of Controlled Dimensions and Divergence: II.
586 Experimental Evaluation of Particle Motion in Aerodynamic Lenses and
587 Nozzle Expansions, Aerosol Science and Technology, 22, 314-324,
588 10.1080/02786829408959749, 1995.
589 Liu, P. S. K., Deng, R., Smith, K. A., Williams, L. R., Jayne, J. T.,
590 Canagaratna, M. R., Moore, K., Onasch, T. B., Worsnop, D. R., and
591 Deshler, T.: Transmission Efficiency of an Aerodynamic Focusing Lens
592 System: Comparison of Model Calculations and Laboratory
593 Measurements for the Aerodyne Aerosol Mass Spectrometer, Aerosol
594 Science and Technology, 41, 721-733, 10.1080/02786820701422278,
595 2007.
596 Loh, N. D., Hampton, C. Y., Martin, A. V., Starodub, D., Sierra, R. G.,
597 Barty, A., Aquila, A., Schulz, J., Lomb, L., Steinbrener, J., Shoeman, R.
598 L., Kassemeyer, S., Bostedt, C., Bozek, J., Epp, S. W., Erk, B., Hartmann,
599 R., Rolles, D., Rudenko, A., Rudek, B., Foucar, L., Kimmel, N.,
600 Weidenspointner, G., Hauser, G., Holl, P., Pedersoli, E., Liang, M.,
601 Hunter, M. S., Gumprecht, L., Coppola, N., Wunderer, C., Graafsma, H.,
602 Maia, F. R. N. C., Ekeberg, T., Hantke, M., Fleckenstein, H., Hirsemann,
603 H., Nass, K., White, T. A., Tobias, H. J., Farquar, G. R., Benner, W. H.,
604 Hau-Riege, S. P., Reich, C., Hartmann, A., Soltau, H., Marchesini, S.,
605 Bajt, S., Barthelmess, M., Bucksbaum, P., Hodgson, K. O., Strüder, L.,
606 Ullrich, J., Frank, M., Schlichting, I., Chapman, H. N., and Bogan, M. J.:

607 Fractal morphology, imaging and mass spectrometry of single aerosol
608 particles in flight, Nature, 486, 513-517, 10.1038/nature11222, 2012.
609 Meinen, J., Khasminskaya, S., Rühl, E., Baumann, W., and Leisner, T.:
610 The TRAPS Apparatus: Enhancing Target Density of Nanoparticle Beams
611 in Vacuum for X-ray and Optical Spectroscopy, Aerosol Science and
612 Technology, 44, 316-328, 10.1080/02786821003639692, 2010.
613 Murphy, D. M., Cziczo, D. J., Froyd, K. D., Hudson, P. K., Matthew, B.
614 M., Middlebrook, A. M., Peltier, R. E., Sullivan, A., Thomson, D. S., and
615 Weber, R. J.: Single - particle mass spectrometry of tropospheric aerosol
616 particles, Journal of Geophysical Research: Atmospheres, 111,
617 10.1029/2006jd007340, 2006.
618 Peck, J., Gonzalez, L. A., Williams, L. R., Xu, W., Croteau, P. L., Timko,
619 M. T., Jayne, J. T., Worsnop, D. R., Miake-Lye, R. C., and Smith, K. A.:
620 Development of an aerosol mass spectrometer lens system for PM2.5,
621 Aerosol Science and Technology, 50, 781-789,
622 10.1080/02786826.2016.1190444, 2016.
623 Schreiner, J., Schild, U., Voigt, C., and Mauersberger, K.: Focusing of
624 Aerosols into a Particle Beam at Pressures from 10 to 150 Torr, Aerosol
625 Science and Technology, 31, 373-382, 10.1080/027868299304093, 1999.
626 Schreiner, J., Voigt, C., Mauersberger, K., McMurry, P., and Ziemann, P.:
627 Aerodynamic Lens System for Producing Particle Beams at Stratospheric
628 Pressures, Aerosol Science and Technology, 29, 50-56,
629 10.1080/02786829808965550, 1998.
630 Srivastava, A., Pitesky, M. E., Steele, P. T., Tobias, H. J., Fergenson, D. P.,
631 Horn, J. M., Russell, S. C., Czerwieniec, G. A., Lebrilla, C. B., Gard, E.
632 E., and Frank, M.: Comprehensive Assignment of Mass Spectral
633 Signatures from Individual Bacillus atrophaeus Spores in Matrix-Free
634 Laser Desorption/Ionization Bioaerosol Mass Spectrometry, Analytical
635 Chemistry, 77, 3315-3323, 10.1021/ac048298p, 2005.
636 Tobias, H. J., Pitesky, M. E., Fergenson, D. P., Steele, P. T., Horn, J.,
637 Frank, M., and Gard, E. E.: Following the biochemical and morphological
638 changes of Bacillus atrophaeus cells during the sporulation process using
639 Bioaerosol Mass Spectrometry, Journal of Microbiological Methods, 67,
640 56-63, 10.1016/j.mimet.2006.03.001, 2006.
641 Wang, X. and McMurry, P. H.: An experimental study of nanoparticle
642 focusing with aerodynamic lenses, International Journal of Mass

643 Spectrometry, 258, 30-36, 10.1016/j.ijms.2006.06.008, 2006.
644 Wang, X., Kruis, F. E., and McMurry, P. H.: Aerodynamic Focusing of
645 Nanoparticles: I. Guidelines for Designing Aerodynamic Lenses for
646 Nanoparticles, Aerosol Science and Technology, 39, 611-623,
647 10.1080/02786820500181901, 2005.
648 Williams, L. R., Gonzalez, L. A., Peck, J., Trimborn, D., McInnis, J.,
649 Farrar, M. R., Moore, K. D., Jayne, J. T., Robinson, W. A., Lewis, D. K.,
650 Onasch, T. B., Canagaratna, M. R., Trimborn, A., Timko, M. T., Magoon,
651 G., Deng, R., Tang, D., de la Rosa Blanco, E., Prévôt, A. S. H., Smith, K.
652 A., and Worsnop, D. R.: Characterization of an aerodynamic lens for
653 transmitting particles greater than 1 micrometer in diameter into the
654 Aerodyne aerosol mass spectrometer, Atmospheric Measurement
655 Techniques, 6, 3271-3280, 10.5194/amt-6-3271-2013, 2013.
656 Wu, X., Omenetto, N., and Winefordner, J. D.: Development,
657 Characterization, and Application of a Versatile Single Particle Detection
658 Apparatus for Time-Integrated and Time-Resolved Fluorescence
659 Measurements—Part I: Theoretical Considerations, Laser Chemistry,
660 2009, 1-10, 10.1155/2009/295765, 2009.
661 Zelenyuk, A., Imre, D., Wilson, J., Zhang, Z., Wang, J., and Mueller, K.:
662 Airborne Single Particle Mass Spectrometers (SPLAT II & miniSPLAT)
663 and New Software for Data Visualization and Analysis in a Geo-Spatial
664 Context, Journal of the American Society for Mass Spectrometry, 26,
665 257-270, 10.1007/s13361-014-1043-4, 2015.
666 Zhang, X., Smith, K. A., Worsnop, D. R., Jimenez, J., Jayne, J. T., and
667 Kolb, C. E.: A Numerical Characterization of Particle Beam Collimation
668 by an Aerodynamic Lens-Nozzle System: Part I. An Individual Lens or
669 Nozzle, Aerosol Science and Technology, 36, 617-631,
670 10.1080/02786820252883856, 2002.
671 Zhang, X., Smith, K. A., Worsnop, D. R., Jimenez, J. L., Jayne, J. T.,
672 Kolb, C. E., Morris, J., and Davidovits, P.: Numerical Characterization of
673 Particle Beam Collimation: Part II Integrated Aerodynamic-Lens–Nozzle
674 System, Aerosol Science and Technology, 38, 619-638,
675 10.1080/02786820490479833, 2004.
676